A COMPLETE CATALOGUE OF LANDSLIDES IN VALLES MARINERIS, MARS. G. Stucky de Quay[1] and P. M. Grindrod[2,3], [1]University College London, Department of Earth Sciences (UCL, Gower Street, London, WC1E 6BT, gaia.quay.10@ucl.ac.uk), [2] Earth and Planetary Sciences, Birkbeck, University of London, UK, [3]Centre for Planetary Sciences, UCL, London, UK.

Introduction: The 4000 km-long rift system in Valles Marineris comprises some of Mars' most dynamic and intriguing surface processes [1]. Although the formation of Valles Marineris has recently been attributed to tectonic processes [2], the subsequent widening of the canyon has occurred as a result of faulting and erosional processes [3]. Landslides are among the most notable features to be found in this system, easily characterized by their distinct scarp and landslide debris morphologies [4]. Landslides have been analyzed individually [5], and in small groups [6,7], although few studies have attempted a complete inventory [8]. In this study, a complete map of every landslide showing a classic debris apron and scarp shape is built, with a focus on measuring and calculating landslide features that will help determine how, when and why these mass movements occurred. The deposit area and source area were calculated, along with the runout length, deposit length, head and base elevation, flow direction, texture, geology, age, slumping, relief, volume, canyon width, and mobility.

Data and Methods: The landslides were identified using mostly Context Camera (CTX), and also High Resolution Stereo Camera (HRSC), with spatial resolutions of 5 m/pixel and 13 m/pixel respectively. For topographical analysis, HRSC data with 100 m/pixel resolution was used. The mapping was conducted in ArcGIS, as were all the spatial analysis measurements. Each chasma was mapped individually, usually by first identifying a deposit and then an associated source area. Only defined debris aprons were used for this study, and as such, large, older, hummocky and slumped landslides with ambiguous and chaotic depositional boundaries were not included in the analysis. A total of 202 landslides are used in this analysis, however the current catalogue approaches 300. Each unique, high-resolution, mapped landslide has an associated 20 variables, which help determine the geomorphological processes that have shaped the canyon in a both local and global scale.

Results: Three types of analyses were used with the data collected from the landslide inventory.

Distribution analysis. Fig. 1 a) shows the locations of the 202 landslides along the canyon, clearly delimiting its walls. The relative area of these landslides is represented in b), and in c) the variation in runout distance is shown. The largest areas can be found in the largest parts of the canyon system such as Melas and Chandor Chasmata, and although this is also true for the runout distances, it has less variation. Lastly, the mobility is also shown in d), which represents the ratio of the runout distance to the total drop height, which represents important lithological properties; these very large mobilities suggest a low coefficient of friction [9]. There is only a variation of 2 orders of magnitude, possibly indicative of the consistent rock properties along Valles Marineris.

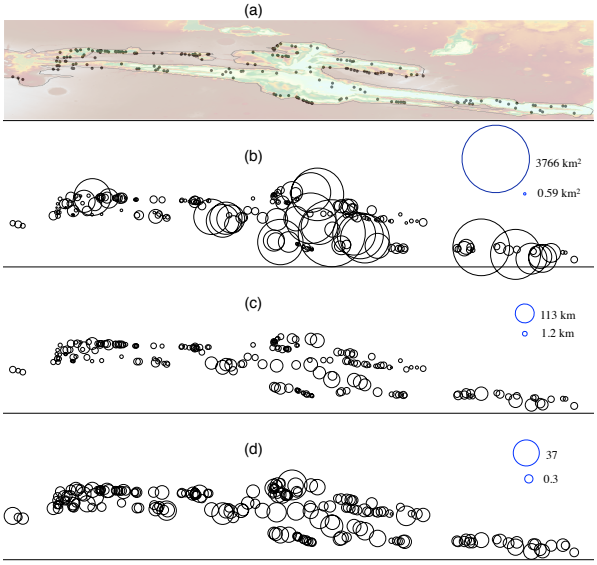

Fig. 1: Four plots showing the landslide characteristics in Valles Marineris. a) shows the locations of the first 202 landslides mapped, over a MOLA elevation model. b) shows the relative variation in area of the landslides, with the maximum and minimum average shown in the scale, and averaging at 200 km^2. In c) we can see the more subdued variation in runout distance, averaging at 20 km between the labeled maximum and minimum. Finally, d) shows the mobility of the landslides and the value range, with a mean of 5.

Regression analysis. In order to better understand the relative importance of variables that were calculated, 4 regression models were made, as seen on Fig. 2. From a) there is a strong correlation between the mapped source area and the deposit area, with a cut-off at 1132 km^2 in source area, and 3766 km^2 in deposit area. The smallest mapped landslide is 0.593 km^2. In plot (b) the volume of each landslide deposit was plotted against its area, in order to understand how these two are related. For landslides with larger areas, the volumes are more uncertain as there is great variation in relief throughout the entire deposit, however it is still possible to discern a correlation. Lastly, in order to understand the role of the canyon's geomorphology

and size in shaping these landslides, the canyon width was plotted against runout and volume. This was done to understand whether a greater amount of canyon floor area would result in longer or greater deposits. The slight upward trend shows that landslide deposits will tend to increase in size when in larger canyons—however, this presents a cause and effect issue, since either factor could have resulted in the other.

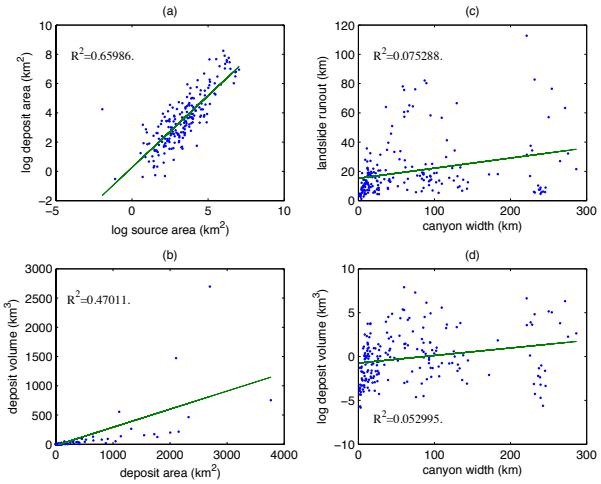

Fig. 2: The four plots show four different regression analyses. (a) and (b) show how the deposit area changes with both the source area and the deposit volume respectively. (c) and (d) show how runout and deposit volume change when a landslide occurs in a larger canyon system, respectively. R-square values are shown for each plot.

Frequency analysis. Histograms for multiple variables were constructed to understand the dominant behaviors of the landslides. Fig. 3 is a rose diagram indicating the direction of flow of the landslide deposits. This was measured by the longitudinal ridges perpendicular to the canyon wall, and for larger deposits with multiple directions, a mean is taken. The plot clearly shows a peak at the NNW and SSE directions, with a large majority of mapped landslides flowing in these directions. The Valles Marineris trough system runs roughly in an E-W direction, such that there is only a small percentage of landslides flowing exactly perpendicular to the overall direction of the canyon, which would be expected from simple gravitational failures. The diagram also shows the very high symmetry of these flows, with many peaks having a symmetrical counterpart, or conversely, with some angles being devoid of almost any landslides.

Conclusions: The initial results of this study show not only geographical variations, but also causal variations with landslide occurrences. The larger landslides in the wide classmate shown in Fig. 1 can be explained by plots (c) and (d) in Fig. 2, which show the relation between canyon width and both runout length and deposit volume. However, this can occur for either one of the following reasons, due to a cause and effect problem: i) the narrower canyons may not allow for larger landslides since these are more confined. Larger canyons would be more prone to have larger deposits since these have an almost unlimited area for the landslides to flow into without confinement; ii) alternatively, it could be that the widening of the chasma could be a consequence of the landslides. The greater volume of mass movements within the central chasmata in Valles Marineris may have contributed to eroding and widening the larger subsystems such as Melas Chasma and Chandor Chasma. Lastly, the flow directions show that gravitational effects are not enough to explain the landslides, and another factor of high symmetry, such as faulting or marsquakes, must be in place. By understanding these mapped variables geographically, temporally, and with respect to other landslide characteristics, it is possible to compare this landslide inventory to the multitude of large inventories that have been built for terrestrial landslides, ultimately helping us know more about these dynamic processes and the conditions required for their emplacement.

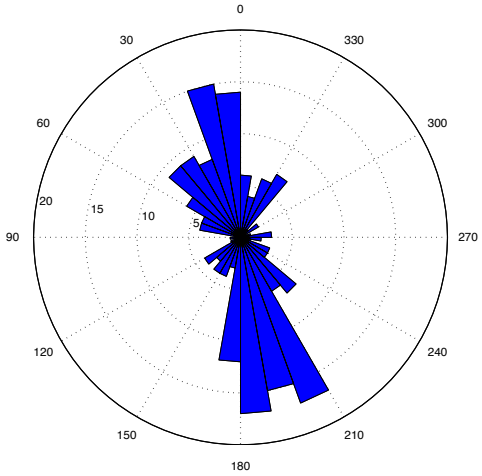

Fig. 3: Rose diagram with 36 bins showing the direction of flow of 202 landslides. The radial values represent the number of landslides within each bin. Each bin consists of 10º.

References: [1] Carr, M. H., Mazurka, H., & Saunders, R. S. (1973) *JGR*, 78(20), 4031-4036. [2] A. Yin. (2012) *Lithosphere*, 4(4):286. [3] Peulvast, J. P., & Masson, P. L. (1993) *Earth, Moon, and Planets*, *61*(3), 191-217. [4] Hooper, D.M, & Smart, K.J. (2013) *LPSC XLIV*, Abstract #1795. [5] Lucchitta, B. K. (1978). *Geol. Soc. of Am. Bulletin*, 89(11), 1601-1609. [6]Shaller, P. J. (1991) *PhD Thesis Caltech*. [7] Quantin, C., Allemand, P., & Delacourt, C. (2004) *Plan. and Space Sci.*, *52*(11), 1011-1022. [8] Crosta, G.B., Frattini, P., Valbuzzi, E. (2013). LPSC XLIV, Abstract #2283. [9] McEwen, A. S. (1989). *Geology*, *17*(12), 1111-1114.